MECHANIKA TEORETYCZNA
I STOSOWANA
Journal of Theoretical
and Applied Mechanics
4, 34, 1996

ON THE THERMAL LUBRICATION THEORY OF TILTING-PAD BEARINGS INCLUSIVE OF PAD BENDING, SIDE LEAKAGE AND INLET PRESSURE BUILD-UP

CZESŁAW M. RODKIEWICZ

Department of Mechanical Engineering University of Alberta

e-mail: cmr@frodo.mece.ualberta.ca

PEIRAN YANG

Qingdao Institute of Architecture and Engineering, Qingdao, P.R.China

Numerical solutions are obtained for the thermo-elastohydrodynamic lubrication of tilting-pad bearings based on the 3-dimensional flow of lubricant. For pressure distribution, a fast Newton-Raphson approach is used in solving the generalized Reynolds equation along with the film thickness and the inlet pressure build-up equations. For temperature distribution, the finite difference method is carried out with the help of a sweeping scheme. The effects of side-leakage are investigated by changing the film geometry parameters. Significant influence is found of the pad's supporting configuration on the modified load carrying capacity and frictional coefficient.

Key words: lubrication theory, thermal effects, side leakage

Notation

$\overline{A}$	–	elastic parameter (defined by Eq (2.11))
B	–	bearing length
b	–	pad thickness
C_1, C_2	–	density-pressure coefficients
C_3	–	density-temperature coefficient
c	–	specific heat of lubricant
D	–	deformation influence coefficient (defined in Eq (3.1))
Ec	–	Eckert number

E_p – Young modulus of pad
F – drag force
h – film thickness
h_c – heat transfer coefficient
h_e – location where the stream lines start to be perpendicular to the moving surface
h_f – film thickness carried by the moving surface at the point far from the leading edge
h_g – geometric film thickness at the leading edge
h_1, h_2 – film thicknesses at the central point of the leading and trailing edges, respectively
k – thermal conductivity of lubricant
k_p – thermal conductivity of pad
L – bearing width
Nu – Nusselt number, $\mathrm{Nu} = h_c B/k_p$
n – coordinate in the direction normal to the pad surface
P – load carrying capacity
Pr – Prandtl number, $\mathrm{Pr} = c\eta_0/k$
p_{in} – inlet pressure at the central point of leading edge
Re – Reynolds number, $\mathrm{Re} = \rho_0 U B/\eta_0$
T, T_p, T_0 – lubricant, pad and ambient temperatures, respectively
U – velocity of the moving surface
u, v – film velocities in the x- and y-directions, respectively
W_p – elastic deformation (bending) of pad
x, y, z – coordinates for film
x_p, y_p, z_p – coordinates for pad
x_c – longitudinal coordinate of the center of pressure
α – viscosity-pressure coefficient
β – viscosity-temperature coefficient
η – viscosity of lubricant
η_0 – ambient viscosity
μ – frictional coefficient
μ_p – Poisson ratio of the pad
ρ – density of lubricant
ρ_0 – ambient density

symbols with a bar indicate dimensionless quantities.

1. Introduction

Oil lubricated tilting-pad bearings are widely used in many types of machines because of their excellent stability, superior durability and high load carrying capacity.

Over decades, numerous works have been done, theoretically or experimentally, to investigate behavior of such bearings from various points of view. As examples we can quote here the recent work of Armentrout and Paquette (1993), Sinha et al. (1993), Earles et al. (1990) and of Abdel-Latif (1988).

It is believed that performance of tilting-pad bearings is affected by many factors, such as the elasticity of bearing components, heat generation and heat transfer, the effect of inlet pressure build-up, etc. As an effort to take most of these factors into analysis, Rodkiewicz and Yang (1995) proposed a numerical solution system, and Yang and Rodkiewicz (1994a) investigated the effects of these factors on performance of centrally pivoted infinitely wide linear pad bearings. In their works the fluid stream was assumed to be 2-dimensional which eliminated the considerations regarding side leakage.

There are many lubrication problems in which side leakage may be neglected. However, it appears that in some circumstances evaluation of the load capacity and of the drag may be subject to significant errors if the side leakage is neglected. For example, this may be the case when considering tilting-pad bearings in high-speed rotating machinery. Present work considers importance of the side leakage in terms of the formulated dimensionless governing parameters.

2. Dimensionless governing equations

Assume that the pad is rectangular in shape with a uniform thickness b. Let the bearing configuration and the coordinate system be as indicated in Fig.1. Let the Newtonian lubricant be of variable density ρ and variable viscosity η. Assume also that the flow is of steady-state and gauge pressure p does not vary across the film thickness h. For such a situation the generalized Reynolds equation proposed by Yang and Wen (1990) together with its associated velocity and velocity gradient equations can be written for the present analysis in the following dimensionless forms

$$\frac{\partial}{\partial \overline{x}}\left[\left(\frac{\overline{\rho}}{\overline{\eta}}\right)_e \overline{h}^3 \frac{\partial \overline{p}}{\partial \overline{x}}\right] + \frac{\partial}{\partial \overline{y}}\left[\left(\frac{\overline{\rho}}{\overline{\eta}}\right)_e \overline{h}^3 \frac{\partial \overline{p}}{\partial \overline{y}}\right] = 6\frac{\partial(\overline{\rho}^*\overline{h})}{\partial \overline{x}} \tag{2.1}$$

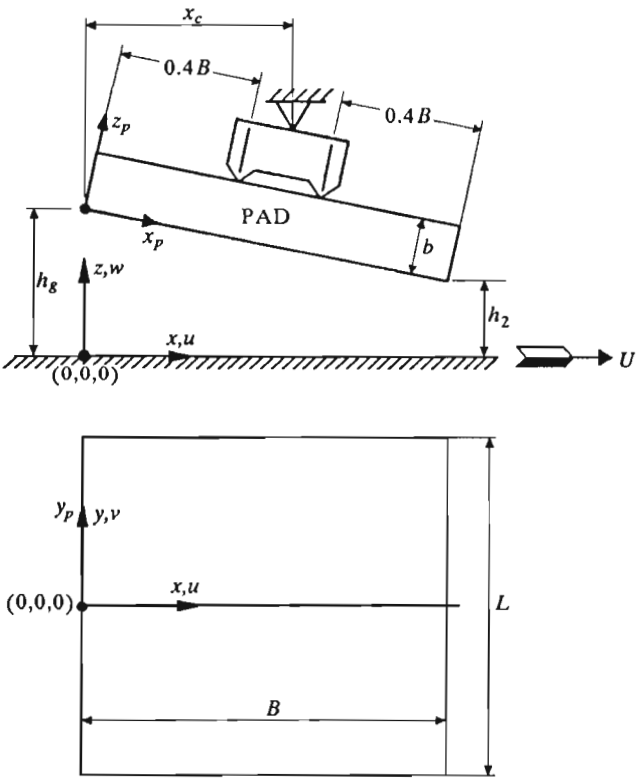

Fig. 1. Basic geometry and coordinate system

$$\overline{u} = 1 + \overline{h}^2 \frac{\partial \overline{p}}{\partial \overline{x}} \Big(\int_0^{\overline{z}} \frac{\overline{z}'\, d\overline{z}'}{\overline{\eta}} - \frac{\overline{\eta}_e}{\overline{\eta}'_e} \int_0^{\overline{z}} \frac{d\overline{z}'}{\overline{\eta}} \Big) - \overline{\eta}_e \int_0^{\overline{z}} \frac{d\overline{z}'}{\overline{\eta}}$$

$$\overline{v} = \overline{h}^2 \frac{\partial \overline{p}}{\partial \overline{y}} \Big(\int_0^{\overline{z}} \frac{\overline{z}'\, d\overline{z}'}{\overline{\eta}} - \frac{\overline{\eta}_e}{\overline{\eta}'_e} \int_0^{\overline{z}} \frac{d\overline{z}'}{\overline{\eta}} \Big) \tag{2.2}$$

$$\frac{\partial \overline{u}}{\partial \overline{z}} = \frac{\overline{h}^2}{\overline{\eta}} \frac{\partial \overline{p}}{\partial \overline{x}} \Big(\overline{z} - \frac{\overline{\eta}_e}{\overline{\eta}'_e} \Big) - \frac{\overline{\eta}_e}{\overline{\eta}}$$

$$\frac{\partial \overline{v}}{\partial \overline{z}} = \frac{\overline{h}^2}{\overline{\eta}} \frac{\partial \overline{p}}{\partial \overline{y}} \Big(\overline{z} - \frac{\overline{\eta}_e}{\overline{\eta}'_e} \Big) \tag{2.3}$$

Where, in the above

$$\left(\frac{\overline{\rho}}{\overline{\eta}}\right)_e = 12\left(\frac{\overline{\eta}_e\overline{\rho}'_e}{\overline{\eta}'_e} - \overline{\rho}''_e\right) \qquad \overline{\rho}^* = 2(\overline{\rho}_e - \overline{\rho}'_e\overline{\eta}_e)$$

$$\overline{\eta}_e = \frac{1}{\int_0^1 \frac{d\overline{z}}{\overline{\eta}}} \qquad \overline{\eta}'_e = \frac{1}{\int_0^1 \frac{\overline{z}\,d\overline{z}}{\overline{\eta}}} \tag{2.4}$$

$$\overline{\rho}_e = \int_0^1 \overline{\rho}\,d\overline{z} \qquad \overline{\rho}'_e = \int_0^1 \left(\overline{\rho}\int_0^{\overline{z}} \frac{d\overline{z}'}{\overline{\eta}}\right) d\overline{z} \qquad \overline{\rho}''_e = \int_0^1 \left(\overline{\rho}\int_0^{\overline{z}} \frac{\overline{z}'\,d\overline{z}'}{\overline{\eta}}\right) d\overline{z}$$

The boundary conditions for Eq (2.1) are given as

$$\begin{aligned} \overline{p}(0,\overline{y}) &= \overline{p}_{in}\left(1 - e^{-\gamma\overline{L}}\right)\left(1 - \frac{4\overline{y}^2}{\overline{L}^2}\right) \\ \overline{p}(1,\overline{y}) &= \overline{p}\left(\overline{x}, \pm\frac{\overline{L}}{2}\right) = 0 \end{aligned} \tag{2.5}$$

where γ is a positive constant; $\overline{p}_{in} = \overline{p}(0,0)$ is the inlet pressure provided by the no-side leakage lubrication theory (Kim and Rodkiewicz (1991))

$$\overline{p}_{in} = \frac{2\mathrm{Re}^*}{\overline{h}_1 + \overline{h}_e}\left(\overline{h}_f - \overline{h}_1\int_0^1 \overline{\rho}_{in}\overline{u}_{in}^2\,d\overline{z}\right) \tag{2.6}$$

When the film shape at the outlet region becomes very divergent due to the elastic deformation of pad, oil cavitation will take place, in such a case the Reynolds boundary condition is applied to the unknown cavitation boundary.

The following dimensionless relationships of viscosity and density with pressure p and temperature T are employed

$$\overline{\eta} = \exp\left[\overline{\alpha}\left(\frac{\mathrm{Ec}}{\mathrm{Re}^*}\right)\overline{p} - \overline{\beta}(\overline{T} - 1)\right] \tag{2.7}$$

$$\overline{\rho} = 1 + \frac{\overline{C}_1\left(\frac{\mathrm{Ec}}{\mathrm{Re}^*}\right)\overline{p}}{1 + \overline{C}_2\left(\frac{\mathrm{Ec}}{\mathrm{Re}^*}\right)\overline{p}} + \overline{C}_3(\overline{T} - 1) \tag{2.8}$$

Furthermore the dimensionless film thickness reads

$$\overline{h}(\overline{x},\overline{y}) = \overline{h}_g - \overline{x}(\overline{h}_g - 1) + \overline{W}_p(\overline{x},\overline{y}) - \overline{W}_p(1,0) \tag{2.9}$$

where $\overline{W}_p$ is the dimensionless bending displacement, which is governed by the following equation

$$\frac{\partial^4 \overline{W}_p}{\partial \overline{x}_p^4} + 2\frac{\partial^4 \overline{W}_p}{\partial \overline{x}_p^2 \partial \overline{y}_p^2} + \frac{\partial^4 \overline{W}_p}{\partial \overline{y}_p^4} = \overline{A}\overline{p}(\overline{x}_p, \overline{y}_p) \tag{2.10}$$

We note that in Eqs (2.9) and (2.10) $\overline{x}$ and $\overline{y}$ are equivalent to $\overline{x}_p$ and $\overline{y}_p$. The constant $\overline{A}$ in Eq (2.10) is given by

$$\overline{A} = \frac{12B^4\rho_0 c T_0(1-\mu_p^2)\mathrm{Ec}}{h_2 E_p b^3 \mathrm{Re}^*} \tag{2.11}$$

The boundary conditions for Eq (2.10) are as follows:

— On edges $\overline{x}_p = 0$ and $\overline{x}_p = 1$

$$\frac{\partial^2 \overline{W}_p}{\partial \overline{x}_p^2} + \mu_p \frac{\partial^2 \overline{W}_p}{\partial \overline{y}_p^2} = 0 \qquad \frac{\partial^3 \overline{W}_p}{\partial \overline{x}_p^3} + (2-\mu_p)\frac{\partial^3 \overline{W}_p}{\partial \overline{x}_p \partial \overline{y}_p^2} = 0 \tag{2.12a}$$

— On edges $\overline{y}_p = \pm\frac{\overline{L}}{2}$

$$\frac{\partial^2 \overline{W}_p}{\partial \overline{y}_p^2} + \mu_p \frac{\partial^2 \overline{W}_p}{\partial \overline{x}_p^2} = 0 \qquad \frac{\partial^3 \overline{W}_p}{\partial \overline{y}_p^3} + (2-\mu_p)\frac{\partial^3 \overline{W}_p}{\partial \overline{x}_p^2 \partial \overline{y}_p} = 0 \tag{2.12b}$$

and at the corner points $\overline{x}_p = 0$, $\overline{y}_p = \pm\frac{\overline{L}}{2}$ and $\overline{x}_p = 1$, $\overline{y}_p = \pm\frac{\overline{L}}{2}$

$$\frac{\partial^2 \overline{W}_p}{\partial \overline{x}_p \partial \overline{y}_p} = 0 \tag{2.12c}$$

For most tilting-pad bearings in engineering, there are mainly two methods to support the pad while allowing it to tilt. Sphere-supported pad can tilt in all directions but rocker-supported pad can tilt in one direction only. In the present study the sphere-supported pad is simulated by fixing 4 points equidistant from the pad center. The rocker-supported pad is simulated by fixing a line at each side of the pad's central line in $\overline{y}$-direction. The former case will be referred here as the "point-supported", whereas the latter as the "line-supported". Consequently, for Eq (2.10) the boundary conditions for the point-supported case and for the line-supported case, respectively, will be as follows

$$\overline{W}_p(0.5 \pm 0.1, \pm 0.1\overline{L}) = 0 \tag{2.12d}$$

$$\overline{W}_p(0.5 \pm 0.1, \overline{y}_p) = 0 \tag{2.12e}$$

The dimensionless temperature of the oil film $\overline{T}$, is described by the following energy equation

$$\mathrm{PrRe}^*\Big\{\overline{\rho u}\frac{\partial \overline{T}}{\partial \overline{x}} + \overline{\rho v}\frac{\partial \overline{T}}{\partial \overline{y}} - \frac{1}{\overline{h}}\Big[\frac{\partial}{\partial \overline{x}}\Big(\overline{h}\int_0^{\overline{z}} \overline{\rho u}\, d\overline{z}'\Big) + \frac{\partial}{\partial \overline{y}}\Big(\overline{h}\int_0^{\overline{z}} \overline{\rho v}\, d\overline{z}'\Big)\Big]\frac{\partial \overline{T}}{\partial \overline{z}}\Big\} =$$

$$= \mathrm{PrEc}\Big[-\frac{\overline{T}}{\overline{\rho}}\frac{\partial \overline{\rho}}{\partial \overline{T}}\Big(\overline{u}\frac{\partial \overline{p}}{\partial \overline{x}} + \overline{v}\frac{\partial \overline{p}}{\partial \overline{y}}\Big)\Big] + \frac{1}{\overline{h}^2}\frac{\partial^2 \overline{T}}{\partial \overline{z}^2} + \mathrm{PrEc}\frac{\overline{eta}}{\overline{h}^2}\Big[\Big(\frac{\partial \overline{u}}{\partial \overline{z}}\Big)^2 + \Big(\frac{\partial \overline{v}}{\partial \overline{z}}\Big)^2\Big] \tag{2.13}$$

and the dimensionless temperature of the pad $\overline{T}_p$ is governed by the Laplace equation; namely

$$\frac{\partial^2 \overline{T}_p}{\partial \overline{x}_p^2} + \frac{\partial^2 \overline{T}_p}{\partial \overline{y}_p^2} + \frac{\partial^2 \overline{T}_p}{\partial \overline{z}_p^2} = 0 \tag{2.14}$$

The boundary conditions for Eqs (2.13) and (2.14) are

$$\begin{aligned} &\overline{T}(0, \overline{y}, \overline{z})\Big|_{\overline{z}\neq 1} = 1 \qquad \text{if} \quad \overline{u}(0, \overline{y}, \overline{z}) \geq 0 \\ &\overline{T}(\overline{x}, \overline{y}, 0) = 1 \qquad\qquad \frac{\overline{k}}{\overline{h}}\frac{\partial \overline{T}}{\partial \overline{z}}\Big|_{\overline{z}=1} = \frac{\partial \overline{T}_p}{\partial \overline{z}_p}\Big|_{\overline{z}_p=0} \\ &-\frac{\partial \overline{T}_p}{\partial \overline{n}} = \mathrm{Nu}(\overline{T}_p - 1)_s \end{aligned} \tag{2.15}$$

From the solution one obtains the load capacity $\overline{P}$, drag $\overline{F}$, frictional coefficient μ and the center of pressure $\overline{x}_c$ by using the following expressions

$$\overline{P} = \int_{-\overline{L}/2}^{\overline{L}/2}\int_0^1 \overline{p}\, d\overline{x} d\overline{y} \tag{2.16}$$

$$\overline{F} = \int_{-\overline{L}/2}^{\overline{L}/2}\int_0^1 \frac{\overline{\eta}\partial \overline{u}}{\overline{h}\partial \overline{z}}\, d\overline{x} d\overline{y} \tag{2.17}$$

$$\overline{\mu} = \frac{\overline{F}}{\overline{P}} \tag{2.18}$$

$$\overline{x}_c = \frac{1}{\overline{P}}\int_{-\overline{L}/2}^{\overline{L}/2}\int_0^1 \overline{xp}\, d\overline{x} d\overline{y} \tag{2.19}$$

In Eqs (2.1) ÷ (2.19) the standard dimensionless parameters are defined as: Prandtl number $\mathrm{Pr} = c\eta_0/k$, Eckert number $\mathrm{Ec} = U^2/(cT_0)$, Reynolds number $\mathrm{Re} = \rho_0 UB/\eta_0$, Nusselt number $\mathrm{Nu} = h_c B/k_p$. The modified Reynolds number $\mathrm{Re}^* = \mathrm{Re}(h_2/B)^2$, is not considered as an independent parameter. Other dimensionless quantities are defined as: $\overline{C}_1 = C_1 c\rho_0 T_0$, $\overline{C}_2 = C_2 c\rho_0 T_0$, $\overline{C}_3 = C_3 T_0$, $\overline{F} = F\mathrm{Re}^*/(\rho_0 U^2 B h_2)$, $\overline{h} = h/h_2$, $\overline{h}_e = h_e/h_2$, $\overline{h}_f = h_f/h_2$, $\overline{h}_g = h_g/h_2$, $\overline{h}_1 = h_1/h_2$, $\overline{k} = (k/k_p)(B/h_2)$, $\overline{L} = L/B$, $\overline{n} = n/B$, n indicates the direction perpendicular to the surface, $\overline{P} = P\mathrm{Re}^*/(\rho_0 U^2 B^2)$, $\overline{p} = p\mathrm{Re}^*/(\rho_0 U^2)$, $\overline{p}_{in} = p_{in}\mathrm{Re}^*/(\rho_0 U^2)$, $\overline{T} = T/T_0$, $\overline{T}_p = T_p/T_0$, $\overline{u} = u/U$, $\overline{v} = v/U$, $\overline{W}_p = W_p/h_2$, $\overline{x} = x/B$, $\overline{x}_c = x_c/B$, $\overline{x}_p = x_p/B$, $\overline{y} = y/B$, $\overline{y}_p = y_p/B$, $\overline{z} = z/h$, $\overline{z}_p = z_p/B$, $\overline{\alpha} = \alpha\rho_0 cT_0$, $\overline{\beta} = \beta T_0$, $\overline{\eta} = \eta/\eta_0$, $\overline{\rho} = \rho/\rho_0$.

3. Numerical technique

An equidistant ($\Delta\overline{x} = \Delta\overline{x}_p = 0.05, \Delta\overline{y} = \Delta\overline{y}_p = 0.05\overline{L}$, $\Delta\overline{z} = 0.1$, $\Delta\overline{z}_p = \overline{b}/4$) mesh is used for the numerical purpose. The iterative procedure contains an outer loop named "T-P-Loop", and two inner loops named "T-Loop" and "P-Loop", respectively. Because of symmetry calculations are made in half of the domain.

Before the program commences the "T-P-Loop" the left side of Eq (2.10) is dispersed with the finite difference method. The coefficient matrix of nodal displacement $\overline{W}_p$ is then inversed, enabling us to express the film thickness at any node (k,l) on the $\overline{x}\overline{y}$ plane as

$$\overline{h}_{k,l} = \overline{h}_g - \overline{x}_k(\overline{h}_g - 1) + \sum_i \sum_j D^{k,l}_{i,j}\overline{p}_{i,j} \tag{3.1}$$

so that nodal film thickness can be coupled with the generalized Reynolds equation, which is solved in the "P-Loop" with a Newton-Raphson approach.

The film temperature $\overline{T}$ and the pad temperature $\overline{T}_p$ are solved simultaneously with the finite difference method in the "T-Loop" where pressure and film thickness are fixed. The system of equations for the nodal temperatures in the film and pad are solved iteratively using a column-by-column application of the conventional tridiagonal matrix algorithm. At every point in the $\overline{x}\overline{y}$ plane, the unknown temperatures at the column of 14 nodes running vertically, from the film through the pad, are solved simultaneously. The sweep starts at the middle point of the bearing leading edge and works toward the corner

of the trailing edge. After a sweep the viscosity, density and velocities, etc., are renewed and a new sweep is then performed. An accuracy for the relative error between two successive sweeps becoming less than 10^{-4} is required.

Details of the numerical technique were presented in a Department Report (Yang and Rodkiewicz (1994b)).

4. Results

The input data common to all solutions include: $B = 0.2\,\mathrm{m}$, $b = 0.032\,\mathrm{m}$, $C_1 = 0.6 \cdot 10^{-9}\,\mathrm{m^2/N}$, $C_2 = 1.7 \cdot 10^{-9}\,\mathrm{m^2/N}$, $C_3 = -6.5 \cdot 10^{-4}\,\mathrm{K^{-1}}$, $c = 2 \cdot 10^3\,\mathrm{J/kgK}$, $E_p = 2.1 \cdot 10^{11}\,\mathrm{N/m^2}$, $h_c = 207\,\mathrm{W/m^2K}$, $h_f = 3 \cdot 10^{-4}\,\mathrm{m}$, $k = 0.14\,\mathrm{W/mK}$, $k_p = 46\,\mathrm{W/mK}$, $T_0 = 313\,\mathrm{K}$, $U = 40\,\mathrm{m/s}$, $\alpha = 1.6 \cdot 10^{-8}\,\mathrm{m^2/N}$, $\beta = 4.2 \cdot 10^{-2}\,\mathrm{K^{-1}}$, $\gamma = 1.6$, $\eta_0 = 0.035\,\mathrm{Ns/m^2}$, $\rho_0 = 8.75 \cdot 10^2\,\mathrm{kg/m^3}$ and $\mu_p = 0.3$. These constitute the following dimensionless parameters: $\overline{b} = 0.16$, $\overline{C}_1 = 0.32865$, $\overline{C}_2 = 0.92188$, $\overline{C}_3 = -0.20345$, $\mathrm{Ec} = 2.556 \cdot 10^{-3}$, $\mathrm{Nu} = 0.9$, $\mathrm{Pr} = 500$, $\mathrm{Re} = 2 \cdot 10^5$, $\overline{\alpha} = 8.764$ and $\overline{\beta} = 13.146$.

The geometry of the oil film is defined by three quantities; namely, h_g, L and h_2. Various values are assigned to them via the corresponding dimensionless parameters; namely, $\overline{h}_g$, $\overline{L}$ and B/h_2 ratio. The dimensionless input data relating to B/h_2 ratio are: $\overline{A} = 6.9539(B/h_2)\mathrm{Ec/Re^*}$, $\overline{h}_e = (B/h_2) \cdot 4.5 \cdot 10^{-3}$, $\overline{h}_f = (B/h_2) \cdot 1.5 \cdot 10^{-3}$, and $\overline{k} = (B/h_2) \cdot 3.0435 \cdot 10^{-3}$.

It is found that the effect of elasticity is weak when B/h_2 ratio is small (i.e. thick film), but it becomes more and more significant as B/h_2 ratio increases. When B/h_2 ratio exceeds 5000, the film becomes so thin and pressure so high that elasticity becomes the dominant factor in the bearing performance. This can be deduced from the results shown in Fig.2 ÷ Fig.7, which were constructed for $B/h_2 = 7500$, $\overline{h}_g = 3$, and $\overline{L} = 1$.

For the point-supported pad, Fig.2 illustrates the distribution of the dimensionless pressure, Fig.3 the surface of the dimensionless film thickness, and Fig.4 the profile of the interface temperature in °C, respectively. For the line-supported pad, the corresponding quantities are given in Fig.5, Fig.6 and Fig.7.

Comparing results of the two cases in question, it is found that the bearing performance strongly depends on the type of pad-support configuration. In the point-support case the pad is deformed with respect to both the $\overline{x}$- and $\overline{y}$-axis. Therefore, under the action of pressure the film thickness surface becomes convex (see Fig.3), which significantly amplifies the side leakage. On

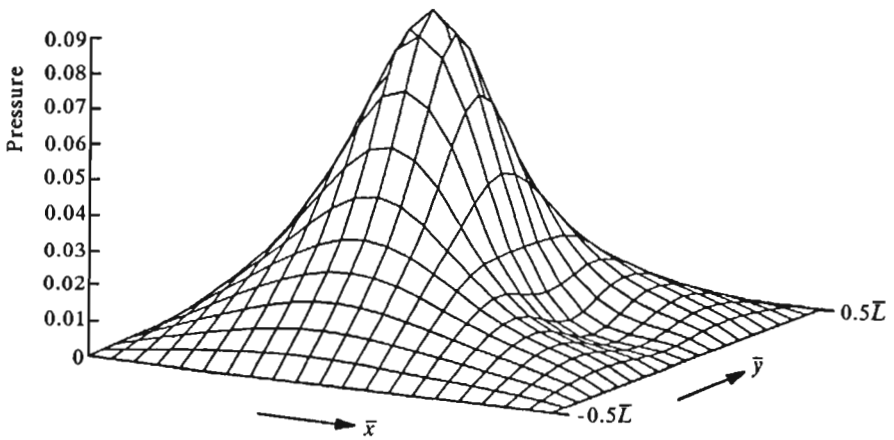

Fig. 2. Dimensionless pressure of a point-supported pad bearing; $B/h_2 = 7500$, $\overline{h}_g = 3, \overline{L} = 1$

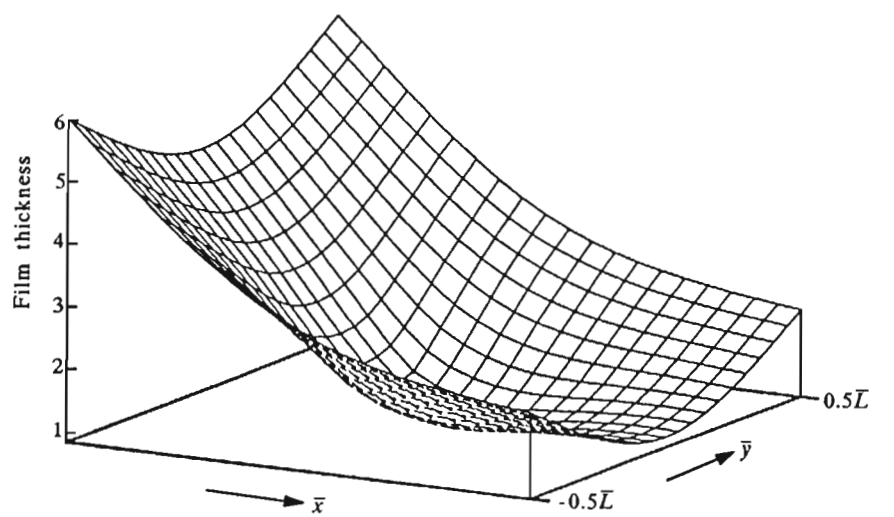

Fig. 3. Dimensionless film thickness for the same case as indicated in Fig.2

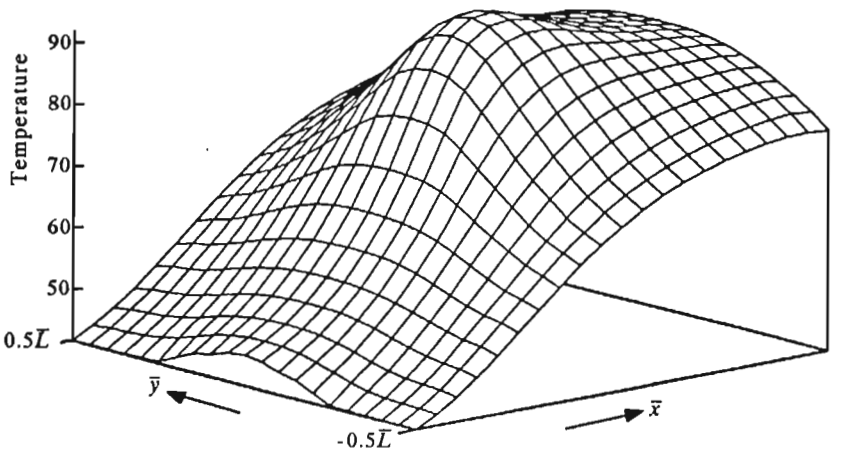

Fig. 4. Interface temperature distribution for the same case as indicated in Fig.2 and Fig.3. Vertical scale is in °C

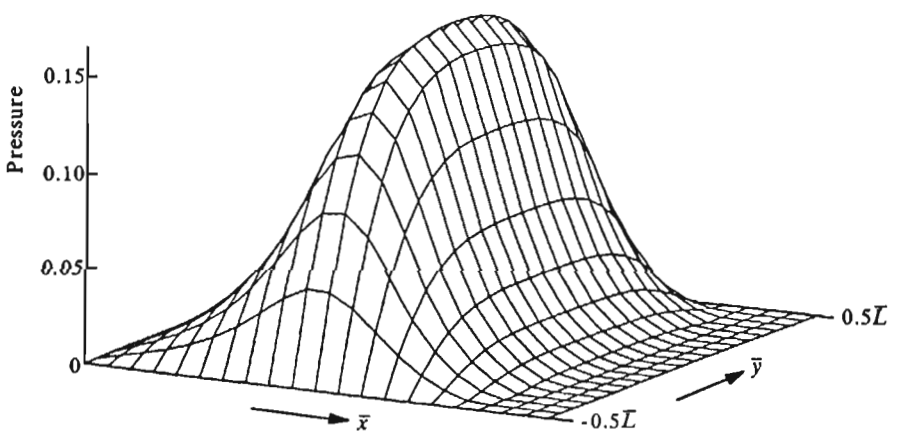

Fig. 5. Dimensionless pressure of a line-supported pad bearing. Parameters are the same as those in Fig.2 ÷ Fig.4

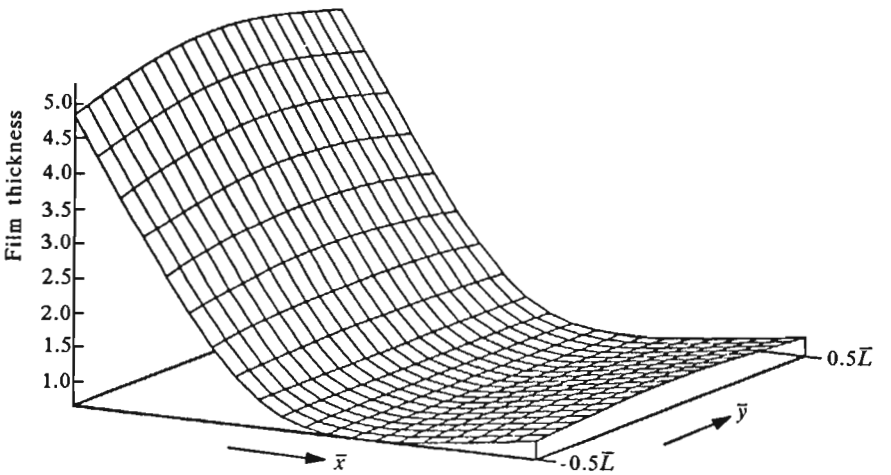

Fig. 6. Dimensionless film-thickness for the same case as indicated in Fig.5

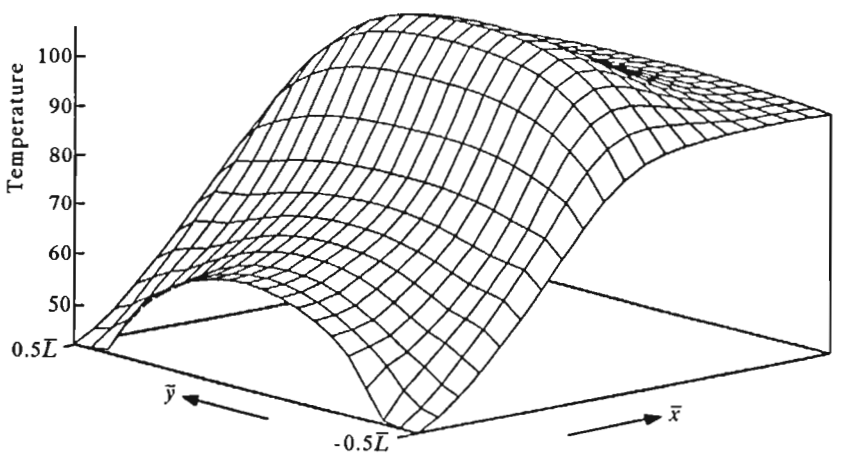

Fig. 7. Interface temperature (°C) for the same case as indicated in Fig.5 and Fig.6

the other hand, in the line-support case the pad is centrally bent upward with respect to the $\overline{y}$-axis only and it is bent slightly downward with respect to the $\overline{x}$-axis (see Fig.6). This, of course, constrains the side leakage, though only to a lesser extent. It should be pointed out that, in the heavily loaded case, because of pad deformation the minimum film thickness is usually located not at the trailing edge but it is somewhere near the pad's center. Furthermore, the minimum film thickness in a point-supported pad bearing is larger than that in a line-supported bearing. For example, $\overline{h}_{min} = 0.835$ (22.3μm) in Fig.3, but it is equal to 0.607 (16.2μm) in Fig.6.

Fig.2 indicates that in the point-supported case pressure develops in the central area of the domain. It drastically decreases in the transverse direction starting immediately at the longitudinal line of symmetry. This phenomenon, no doubt, is caused by the divergency of the film profiles toward the pad sides. Fig.5, however, shows quite different interrelationship. Here pressure is high in the transverse direction extending to locations close to the sides. It is interesting to notice that, not only the distributions shown in Fig.2 and Fig.5 are different, but also the maximum pressures are different; namely, in the point-supported case $\overline{p}_{max} = 0.09095$ ($p_{max} = 35.81$ MPa) whereas in the line-supported case $\overline{p}_{max} = 0.1673$ ($p_{max} = 65.87$ MPa).

It is also very interesting to see from Fig.4 and Fig.7 that, high pressure is always associated with high temperature, but low pressure is not necessarily associated with low temperature. Taking the reverse-flow region as an example, we note that pressure there is very low but the interface temperature is relatively high, especially in the line-supported case (see the "arch" shaped profile in the central part of the leading edge in Fig.7).

The unit-width load carrying capacity $\overline{P}/\overline{L}$ is found strongly depends on the pad-support configurations and the bearing width $\overline{L}$. This can be seen from Fig.8 where curves labeled number 1 represent line-support, whereas number 2 point-support. Similar tendencies can be observed for various $\overline{h}_g$ parameters.

For narrow pads ($\overline{L} = 0.5$) both configurations offer almost the same low values of load capacity. This is because narrow pads are not easily bent with respect to the $\overline{x}$-axis. For the line-supported pad bearing, $\overline{P}/\overline{L}$ increases rapidly as $\overline{L}$ increases over the full range from 0.5 to 2.0. Obviously for such a configuration bending of pad with respect to the $\overline{x}$-axis is constrained, so that for wider pads the side leakage becomes smaller. For the point-supported pad bearing, however, the variation of $\overline{P}/\overline{L}$ is not monotonous. As $\overline{L}$ increases $\overline{P}/\overline{L}$ at first increases, reaches its maximum at $\overline{L}$ around unity, and then rapidly decreases. Such a decrease of $\overline{P}/\overline{L}$ obviously comes from the more and more significant side leakage. It is amplified in the point-supported case

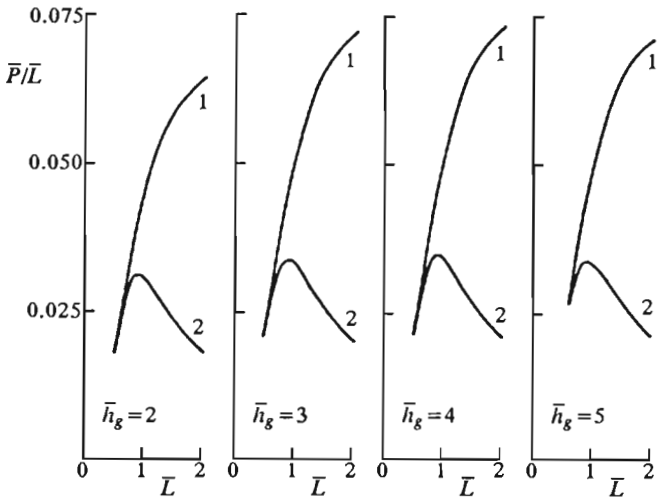

Fig. 8. Variations of $\overline{P}/\overline{L}$ versus $\overline{L}$ for various $\overline{h}_g$; $B/h_2 = 4000$, 1 – line-supported, 2 – point-supported

by the large bending displacements off the pad with respect to the longitudinal axis.

In order to show the effects of B/h_2 ratio on the load capacity for different pad-support configurations, Fig.9 is constructed. Here variations of $\overline{P}/\overline{L}$ are depicted versus B/h_2 for square pads ($\overline{L} = 1$) working at $\overline{h}_g\ 3 = 3$. The decrease of $\overline{P}/\overline{L}$ with increasing B/h_2 is mainly caused by the increase of film temperature. Larger is the B/h_2 ratio smaller is the film thickness and higher is the temperature. As temperature increases viscosity of lubricant decreases, and therefore pressure decreases, and consequently load capacity decreases. The pad deformation with respect to the $\overline{y}$-axis is beneficial to the load capacity. In the line-supported case, when B/h_2 reaches about 4000, some kind of equilibrium appears to be reached between the negative effect of high temperature and the positive effect of large deformation. This equilibrium, however, is broken when B/h_2 approximately equals 4300 at which state the oil cavitation, occurswhich commences at the trailing edge. Cavitation reduces the load supporting area so that as B/h_2 further increases, $\overline{P}/\overline{L}$ decreases again until B/h_2 ratio is approximately equal to 7500 at which state cavitation has fully developed and another equilibrium is observed. In the point-supported case the variation of $\overline{P}/\overline{L}$ against B/h_2 shows a quite different characteristic. Now as B/h_2 increases the positive effect of pad bending, with respect to the $\overline{y}$-axis, is somehow eliminated by the negative

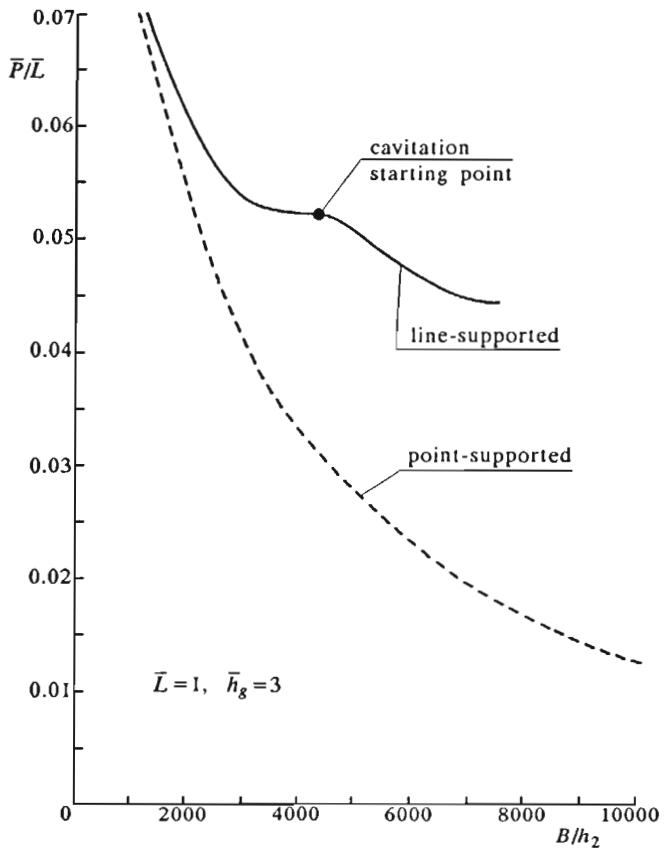

Fig. 9. Variations of $\overline{P}/\overline{L}$, versus B/h_2; $\overline{L} = 1$, $\overline{h}_g = 3$

effect of pad bending with respect to the $\overline{x}$-axis. So the $\overline{P}/\overline{L}$ ratio decreases monotonically throughout the whole range of B/h_2 ratios.

The effect of the inlet pressure build-up on the load capacity is always positive, but it is of significance only when B/h_2 ratio is small, and it is negligible when B/h_2 ratio becomes sufficiently large (approximately, $B/h_2 \geq 6000$). The contribution of the inlet pressure build-up can be understood by referring to Table 1, where the ratio of the maximum inlet pressure to the maximum film pressure is given for the cases shown in Fig.9.

Table 1. Values of $\overline{p}(0,0)/\overline{p}_{max}$ for $\overline{L} = 1, \overline{h}_g\ 3 = 3$

B/h_2	$\overline{p}(0,0)/\overline{p}_{max}$	
	point-supported	line-supported
1000	0.2075	0.2049
1500	0.1644	0.1580
2000	0.1319	0.1213
2500	0.1081	0.0939
3000	0.0882	0.0711
3500	0.0710	0.0522
4000	0.0572	0.0383
4500	0.0459	0.0289
5000	0.0374	0.0226
5500	0.0310	0.0185
6000	0.0262	0.0155
6500	0.0224	0.0131
7000	0.0194	0.0110
7500	0.0170	0.0090
8000	0.0150	–
8500	0.0134	–
9000	0.0120	–
9500	0.0109	–
10000	0.0098	–

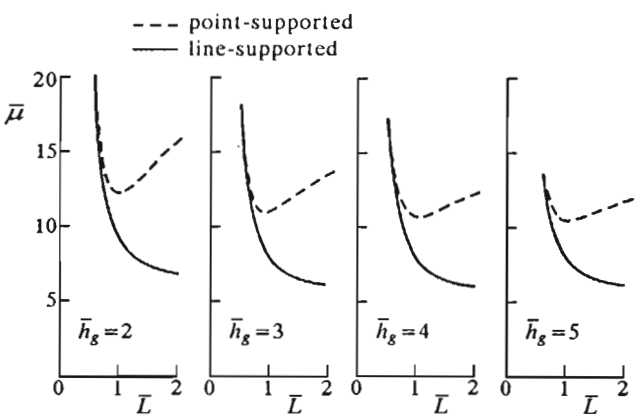

Fig. 10. Variations of μ versus $\overline{L}$; $B/h_2 = 4000$

Fig.10 illustrates variations of the frictional coefficient $\overline{\mu}$ (defined by Eq

(2.18)) versus the pad width $\overline{L}$ for different values of $\overline{h}_g$. Again we find that the line-supported configuration is superior to the point-supported one. Similarly to what was said regarding the load capacity, in the point-supported case the optimum value of $\overline{L}$ for the minimum frictional coefficient is also around unity.

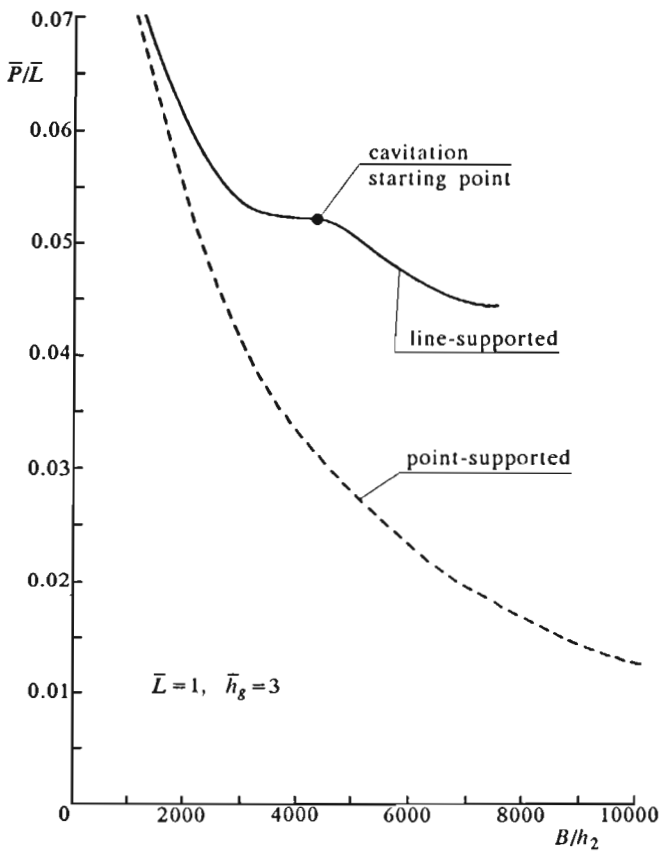

Fig. 11. Variations of $\overline{\mu}$ and $\overline{F}$ versus B/h_2; $\overline{L} = 1, \overline{h}_g = 3$

For parameters $\overline{L} = 1$ and $\overline{h}_g\ 3 = 3$, the dimensionless drag force $\overline{F}$ (defined by Eq (2.17)) and frictional coefficient $\overline{\mu}$ are depicted against B/h_2 ratio in Fig.11. The similarity of the curves of $\overline{F}$ in Fig.11 to the curves of $\overline{P}/\overline{L}$ in Fig.9 is evident because that shear stress is closely related to pressure. Comparison of the line-supported $\overline{P}/\overline{L}$ curve in Fig.9, however, with the corresponding $\overline{F}$ curve in Fig.11 is somehow simpler. The first equilibrium shown in Fig.9 can not be found in Fig.11.

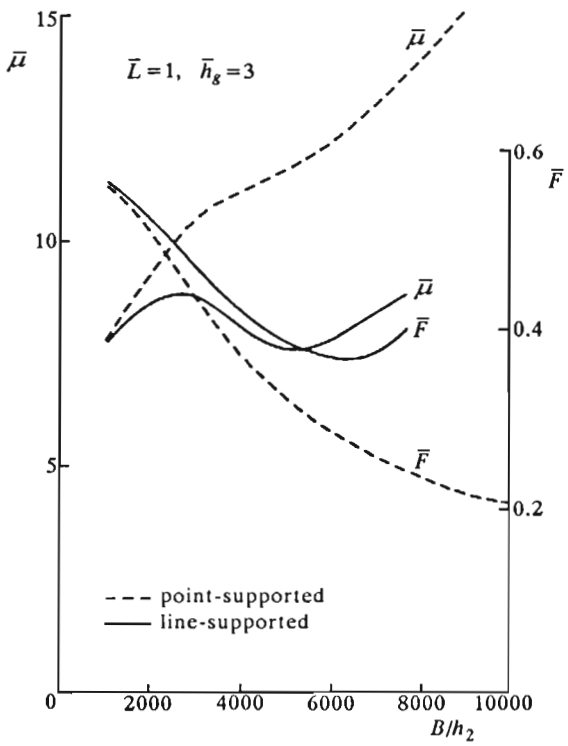

Fig. 12. Variations of $\bar{x}_c$ versus $\bar{h}_g$

The information regarding the location of the center of pressure is of great importance for bearing design. The supporting point should coincide with the center of pressure. Fig.12 shows the variations of the center of pressure $\bar{x}_c$, in terms of the $\bar{h}_g$ parameter. Corresponding to Fig.12 the load capacity and frictional coefficient have been presented in Fig.8 and Fig.10, respectively. It is known that, according to the classical lubrication theory, $\bar{x}_c$ could not be equal to or less than 0.5. But, the present results reveal that, the geometric center or central line may be the most suitable position for supporting the pads. In Fig.12, for $\bar{x}_c = 0.5$, the horizontal coordinates of all curves fall into the most useful region of $\bar{h}_g$ parameter, i.e., $2.5 < \bar{h}_g < 4$. Fig.13 shows the variations of $\bar{x}_c$ versus B/h_2. Corresponding to these curves the load and drag have been presented in Fig.9 and Fig.11, respectively. From the curves we know that, for large B/h_2 ratio, the location of the center of pressure moves even upward. Two reasons can be suggested to explain this phenomenon. Firstly, the present analysis is considering thermal effects. Since the temperature in

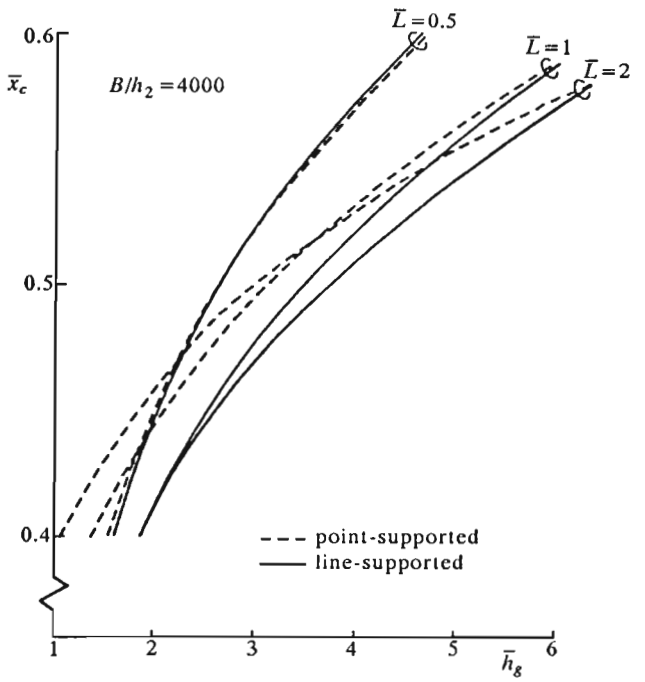

Fig. 13. Variations of $\bar{x}_c$ versus B/h_2

the inlet region is always lower than that in the outlet region, so comparing with the existing isothermal theory, the center of pressure will move upward. Secondly, the bending of pad changes shape of the oil film, resulting in the upward movement of the center of pressure also.

5. Conclusions

1. The thermo-elastohydrodynamic lubrication of finite width tilting-pad bearings is solved numerically. All governing equations are expressed in dimensionless forms, which yields the dimensionless problem parameters.

2. The results are focused on the influence of side leakage. It is found that the bending of pad with respect to the $\bar{y}$-axis is beneficial to the bearing performance, because it usually increases the wedge effect. It is also found that, in the point-supported case the bending of pad with

respect to the $\overline{x}$-axis is detrimental to the bearing performance because it enhances the side leakage.

3. According to the obtained results it is recommended that the line-supported pad configuration be adopted for bearing design, if possible. And, in the case the point-supported pad is required, it is recommended that square pad be used and be supported at its geometric center.

Acknowledgements

This work is financially supported by the Natural Sciences and Engineering Research Council of Canada in the form of grant A-4198 (Rodkiewicz), and partly by the National Natural Science Foundation of China (Yang). The authors also wish to express their thanks to Ms. Gail Anderson for carefully typesetting the manuscript.

References

1. ABDEL-LATIF L.A., 1988, Analysis of Heavily Loaded Tilted Pad Thrust Bearings with Large Dimensions under TEIID Conditons, *ASME Journal of Tribology,* **110**, 467-476
2. ARMENTROUT R.W., PAQUETTE D.J., 1993, Rotordynamic Characteristics of Flexure-Pivot Tilting-Pad Journal Bearings, *STLE Tribology Transactions,* **36**, 443-451
3. EARLES L.L., PALAZZOLO A.B., ARMENTROUT R.W., 1990, A Finite Element Approach to Pad Flexibility Effects in Tilt Pad Journal Bearings: Part 1: Single Pad Analysis, *ASME Journal of Tribology,* **112**, 169-176
4. KIM K.W., RODKIEWICZ C.M., 1991, On the Thermal Effects in the Design of Tilting-Pad Bearings Subjected to Inlet Pressure Build-Up, *ASME Journal of Tribology,* **113**, 526-532
5. RODKIEWICZ C.M., YANG P., 1995, Proposed TEIIL Solution System for the Thrust Bearings Inclusive of Surface Deformations, *STLE Tribology Transactions,* **38**, 1, 75-85
6. SINHA A.N., ATHRE K., BISWAS S., 1993, Spring-Supported Hydrodynamic Thrust Bearing with Special Reference to Elastic Distortion Analysis, *Tribology International,* **26**, 251-263
7. YANG P., RODKIEWICZ C.M., 1994a, The Effects of Temperature, Elasticity and Fore-Region Pressure Build-Up on Performance of Centrally Pivoted Linear Pad Bearings, *Tribology International,* **27**, 5, 331-341
8. YANG P., RODKIEWICZ C.M., 1994b, On the Proposed TEHL Solution System for Tilting-Pad Bearings Inclusive of Pad Bending and Side Leakage, Department Report No.92, Department of Mechanical Engineering, University of Alberta, Canada

9. YANG P., WEN S., 1990, A Generalized Reynolds Equation for Non-Newtonian Thermal Elastohydrodynamic Lubrication, *ASME Journal of Tribology*, **112**, 631-636

Termiczna teoria smarowania łożyska ślizgowego z uwzględnieniem odkształceń płytek, upływów bocznych i ciśnienia zasilania

Streszczenie

W pracy podano numeryczne rozwiązanie zagadnienia termo-elastohydrodynamicznego smarowania dla łożyska ślizgowego z wahliwymi płytkami. Uwzględniono trójwymiarowy przepływ smaru. Dla wyznaczenia rozkładu ciśnienia na podstawie uogólnionego równania Reynoldsa zastosowano szybką metodę Newtona-Raphsona. *Dla wyznaczenia rozkładu temperatury posłużono się metodą różnic skończonych.* Efekt upływu bocznego zbadano zmieniając parametry geometryczne warstwy smaru. Wykazano, że sposób podparcia płytek ma istotny wpływ na nośność łożyska i współczynnik oporów ruchu.

Manuscript received November 22, 1995; accepted for print May 21, 1996